Dynamic ^{18}F-FDG PET Lymphography for In Vivo Identification of Lymph Node Metastases in Murine Melanoma

Hannah Lockau[1–3], Volker Neuschmelting[2], Anuja Ogirala[1,2], Antoni Vilaseca[1,2], and Jan Grimm[1,2,4,5]

[1]Molecular Pharmacology Program, Memorial Sloan Kettering Cancer Center, New York, New York; [2]Department of Radiology, Memorial Sloan Kettering Cancer Center, New York, New York; [3]Department of Radiology, University Hospital Cologne, Cologne, Germany; [4]Pharmacology Program, Weill Cornell Medical College, New York, New York; and [5]Department of Radiology, Weill Cornell Medical College, New York, New York

Positron lymphography using ^{18}F-FDG followed by Cerenkov-guided resection of lymph nodes in healthy mice has previously been introduced by our group. Our aim in this study was to further assess the technique's potential beyond merely localizing sentinel lymph nodes. We now aimed to evaluate the potential of positron lymphography to characterize the nodes with respect to their tumor status in order to identify metastatic lymph nodes. We explored whether metastatic nodes could be distinguished from normal nodes via dynamic ^{18}F-FDG lymphography, to then be resected under Cerenkov imaging guidance. **Methods:** A murine melanoma cell line highly metastatic to lymph nodes (B16F10) was implanted subcutaneously on the dorsal hind paw of C57 mice while the tumor-free contralateral leg served as an intraindividual control. A model of reactive lymph nodes after concanavalin A challenge served as an additional control to provide nonmalignant inflammatory lymphadenopathy. Dynamic PET/CT imaging was performed immediately after injection of ^{18}F-FDG around the tumor or intracutaneously in the contralateral footpad. Furthermore, PET/CT and Cerenkov studies were performed repeatedly over time to follow the course of metastatic spread. In selected mice, popliteal lymph nodes underwent Cerenkov luminescence imaging. Hematoxylin and eosin staining was done to verify the presence of lymphatic melanoma infiltration. **Results:** Positron lymphography using ^{18}F-FDG was successfully performed on tumor-bearing and non–tumor-bearing mice, as well as on controls bearing sites of inflammation; the results clearly identified the sentinel lymph node basin and delineated the lymphatic drainage. Significantly prolonged retention of activity was evident in metastatic nodes as compared with controls without tumor. On the basis of these results, the contrast in detection and identification of metastatic lymph nodes was distinct and could be used for guided lymph node resection, such as by using Cerenkov luminescence imaging. However, retention after ^{18}F-FDG lymphography was also seen in acute inflammatory lymphadenopathy. **Conclusion:** In a tumor model, significantly longer retention of the radiotracer during ^{18}F-FDG lymphography was seen in metastatic than nonmetastatic lymph nodes, allowing for differentiation between the two and for selective resection of tumor-bearing nodes using Cerenkov imaging. Inflammation can be better differentiated in a subacute state.

Key Words: sentinel lymph node; positron lymphography; Cerenkov; melanoma; metastasis

J Nucl Med 2018; 59:210–215
DOI: 10.2967/jnumed.117.196303

In melanoma, sentinel lymph node status has proven to be a critical prognostic factor in the prediction of disease-free survival, and thus sentinel node biopsy has been implemented in the routine clinical workup (*1,2*). Throughout primary tumor growth and preceding metastasis formation, the lymphatic vascular drainage system and downstream tumor-draining lymph nodes undergo extensive structural tumor- and tumor microenvironment–induced alterations. With gradual recruitment of the lymphatic system by a tumor, consecutive hypertrophy of the associated lymph vessels and lymphatic sinuses, as well as early hypertrophy of tumor-draining lymph nodes, is seen, and consequently lymphatic flow from the tumor site into the draining lymph basin is promoted.

To date, pre- and intraoperative sentinel lymph node diagnostics are limited to nonspecific identification of the first tumor-draining lymph node by means of lymphoscintigraphy using ^{99m}Tc-radiocolloid or optical guidance by interstitial administration of isosulfan blue or fluorescent dyes. Both techniques have clear advantages such as widespread availability and direct optical guidance in surgery but have their major limitation in the inability to give any evidence about potential metastatic involvement or consecutive alterations in lymph flow dynamics before lymph node excision. Current research tries to fill in that diagnostic gap, and some approaches already have shown promising results (*3*). New developments comprise selective molecular imaging probes that enable detection of metastases in low cell stages in vivo (*4,5*), as well as imaging modalities bearing features to also detect the sentinel node intraoperatively, such as by optical means (*5*). Tumor-induced alterations in lymphatic drainage have successfully been visualized previously by MRI using gadolinium nanoparticles or in a longitudinal near-infrared fluorescence imaging study in mice (*6*). Of note, translation into the clinic remains tedious for most of these novel techniques and agents because of regulatory requirements.

We have shown in prior studies that positron lymphography using ^{18}F-FDG can identify the draining lymph nodes (*7*) and that in vivo Cerenkov luminescence imaging in humans with the PET

Received May 31, 2017; revision accepted Aug. 25, 2017.
For correspondence or reprints contact: Jan Grimm, Department of Radiology, Memorial Sloan Kettering Cancer Center, Sloan Kettering Institute, ZRC-2025, 417 E. 68th St., New York, NY 10065.
E-mail: grimmj@mskcc.org
Published online Sep. 14, 2017.

tracer ^{18}F-FDG is feasible (*8*). We aimed to further explore the usefulness of positron lymphography as a possible diagnostic tool not only for localization of lymph nodes but also for characterization of their tumor status, that is, to identify tumor-bearing lymph nodes, visualize tumor-induced lymph flow alterations, and evaluate the possibility for intraoperative Cerenkov-guided selective resection of tumor-positive nodes.

MATERIALS AND METHODS

Animal Experiments

All animal procedures were performed under general 2% isoflurane–air inhalation anesthesia in compliance with the Institutional Animal Care and Use Committee guidelines as well as the Guide for the Care and Use of Laboratory Animals from the National Institutes of Health.

The animals were euthanized at a primary tumor diameter of more than 1 cm or the occurrence of tumor-related complications such as signs of pain or distress, weight loss, gait change, bleeding, skin ulceration, or tumor necrosis.

Melanoma Lymph Node Metastasis Model. Nine 6- to 8-wk-old B6N-Tyr$^{c\text{-}Brd}$/BrdCrCrl mice (Charles River Laboratories Inc.) received, on the dorsal right hind paw, a subcutaneous implant of 2×10^5 B16F10 melanoma cells suspended in 10 μL of Matrigel (Corning Life Sciences). The mice developed ipsilateral melanoma lymph node metastases within 4 wk. If the primary tumor exceeded 8 mm in diameter within the first 21 d, tumor-reduction surgery was performed to allow for further metastatic growth and maximize the yield of lymph node metastases. The popliteal lymph nodes draining the contralateral hind leg served as a healthy intraindividual control. After imaging, the mice were euthanized and metastatic lymph nodes were harvested for exemplary hematoxylin and eosin (H&E) staining.

Acute Inflammatory Lymphadenitis. Four albino B6 mice were injected with a 100-μg mixture of concanavalin A and 20 μL of phosphate-buffered saline (Sigma-Aldrich) on the right hind paw to induce acute lymphadenitis (*5,9*). ^{18}F-FDG lymphography was performed 3 h after injection (early inflammation), 24 h after injection (peak inflammation), and 120 h after injection (resolving inflammation). The mice were then euthanized, and inflammatory lymph nodes were harvested for histologic examination by H&E staining.

^{18}F-FDG PET/CT Imaging and Image Postprocessing

For dynamic ^{18}F-FDG PET/CT imaging, an Inveon small-animal PET/CT scanner (Siemens Preclinical Solutions) was used. The mice were kept fasting for 4 h and then positioned prone on the built-in animal bed. ^{18}F-FDG was supplied by IBA Molecular and acquired through the on-site radiopharmacy (specific activity > 41 MBq/mmol, radiochemical purity > 98%). Approximately 3.33–4.07 MBq of ^{18}F-FDG in a total volume of up to 10 μL were injected intracutaneously around the site of the tumor or inflammation and in the contralateral healthy hind paw. Dynamic PET imaging over a 30-min time frame was immediately commenced (delay from injection to scan, <120 s). The preset PET energy window was 350–700 keV, and the coincidence-timing window was 6 ns. After acquisition, image data were corrected for detector nonuniformity, dead-time count losses, positron branching ratio, and physical decay. Corrections for attenuation, scatter, and partial-volume averaging were not applied. Counting rates in the reconstructed images were converted to activity concentrations in percentage of injected dose per gram of tissue, using a system calibration factor (μCi/mL/cps/voxel) derived from imaging a mouse-sized water-equivalent phantom containing ^{18}F.

To provide an anatomic reference, a whole-body CT scan was obtained using a standardized scan protocol with a preset voltage of 80 kV and an anode current of 500 μA. One hundred twenty rotational steps were performed for a total of 220°, and the approximate scan time was 120 s with an exposure time of 145 ms/frame.

For further dynamic analysis of PET images, dynamic reconstruction in 1-min steps was performed. Time–activity curves were then created using ASIProVM (Concorde Microsystems) software by drawing elliptic regions of interest on multiple consecutive slices to create a spheric volume of interest, visually outlining the borders of each individual lymph node and calculating the absolute volume in cubic millimeters.

For reconstruction of the axial ^{18}F-FDG PET/CT images at lymph node level, OsiriX imaging software (version 5.5.1; Pixmeo) was used. For further illustration and to facilitate visual outlining of lymphatic drainage, fused 3-dimensional maximum-intensity-projection images were generated using the manufacturer's analysis software, Inveon Research Workspace (Siemens Preclinical Solutions).

Cerenkov Luminescence Imaging

After ^{18}F-FDG lymphography (~2 h after injection), the IVIS Spectrum (Perkin-Elmer) preclinical imaging system equipped with a cryo-cooled charge-coupled-device camera was used for Cerenkov-guided resection of metastatic nodes in a euthanized B6/albino mouse. After removal of the fur and skin, the mouse was positioned prone in the dedicated imaging chamber and sequential 5-min acquisitions were obtained during stepwise surgical exposure and resection of metastatic and contralateral healthy popliteal lymph nodes. Injection sides were placed outside the field of view for better demarcation of the low-intensity Cerenkov luminescence signal. Using the manufacturer's software, region-of-interest analysis was performed on each leg to obtain average radiance values in p/s/cm^2/sr, outlining the lymph node and the adjacent exposed muscular tissue separately for respective comparison with background values. Signal-to-background ratios were then calculated for each leg.

Statistical Analysis

For all statistical analyses, Prism software (version 7.0; GraphPad) was used. To allow for comparability and to account for the intra- and interindividually highly variant lymphatic uptake and drainage, group analyses of activity concentrations were performed after data normalization to the intraindividual peak lymphatic uptake in either of the nodes or to the peak uptake of the intraindividual healthy node, respectively. A 20-min period starting at each individual lymph node's time point of peak uptake was then used for further analysis.

Data are displayed as mean values ± SDs. Paired 2-tailed *t* tests were performed to compare grouped activity ratios at peak uptake versus 20 min after peak. Unpaired *t* tests were performed to compare activity ratios between metastatic and inflammatory nodes in different inflammation states (early/peak/resolving) in reference to their respective intraindividual healthy control nodes at the 20-min-after-peak time point. Unpaired *t* tests were also performed to test grouped ^{18}F-FDG lymphography time–activity curves for significant differences in relative activities among healthy versus metastatic nodes. The significance level was set at a P value of less than 0.05.

RESULTS

Image-Based Lymph Node Differentiation

In mice implanted with B16F10 tumors, ^{18}F-FDG lymphography by dynamic PET/CT imaging could successfully be performed on both tumor-bearing and contralateral non–tumor-bearing legs. Bilaterally, major draining lymphatic vessels, as well as the popliteal lymph node as the first draining, or sentinel, node for the hind paw, could be visualized in all mice ($n = 9$). Because of the approximately 2-min delay from injection to initiation of the scan, very early drainage phases were not recorded, yet there was already evidence of ^{18}F-FDG in the sentinel nodes in all mice within the first scan minute, indicating fast lymphatic drainage. ^{18}F-FDG drainage or substantial uptake into higher-echelon nodes or other lymphatic sites was not evident within the imaging time frame of 30 min. Pooled activity remained evident at both injection sites.

Within 30 min, the systemic ^{18}F-FDG signal increased because of expected diffusion into the vasculature at the site of injection and possibly also through lymphatic transition into the blood circulation. In our mouse model, there was no evidence of metastatic spread to sites other than the first tumor-draining node basin on whole-body images or macroscopic necropsy thereafter.

Comparison of the normalized time–activity curve of the metastatic and corresponding healthy popliteal lymph nodes in 9 mice revealed significant differences in ^{18}F-FDG dynamics. At the time of peak activity, the mean ratio between the normalized activities in the corresponding metastatic and healthy nodes was near 1, indicating no relevant difference in uptake (1.08 ± 0.93; $n = 9$). However, 20 min after peak activity, the mean activity ratio was more than double the ratio at peak activity because of differential retention of activity in metastatic nodes (2.41 ± 1.03; $n = 9$; $P < 0.01$) (Fig. 1).

To further specify the dynamics of the uptake, a grouped analysis of normalized time–activity curves was performed, evaluating the decline in activity over 20 min from the peak activity in individual lymph nodes. At peak, mean relative activity values were marginally higher in healthy nodes, at 0.84 (±0.16) versus 0.74 (±0.04) in metastatic nodes ($P > 0.05$). No significant difference was seen between healthy and metastatic lymph nodes within the first 12 min of image acquisition (Figs. 1 and 2). However, from minute 13, retention of ^{18}F-FDG over the evaluated time course was significantly higher in metastatic lymph nodes than in healthy contralateral control nodes, resulting in statistically different residual mean relative activity values ($P < 0.05$) (Fig. 1). Fast reduction (washout) of activity was seen in the healthy nodes. Even in a lymph node with only small melanoma cell infiltrates mainly on the lymph node border, activity curves in the metastatic and healthy nodes tended to diverge later in the scan, showing a retention effect in the diseased node. Figure 2 illustrates this finding in comparison to activity curves obtained from a mouse bearing a large lymph node metastasis.

The volume of metastatic nodes significantly correlated with the retained relative activity at 20 min after peak ($P < 0.05$; linear regression coefficient $r^2 = 0.61$, $n = 9$), as illustrated in Supplemental Figure 1 (supplemental materials are available at http://jnm.snmjournals.org). Increasing volume led to increasing ^{18}F-FDG retention normalized per gram of tissue. There was no correlation between node volume and the corresponding retained relative activity values observed in healthy nodes ($P > 0.1$).

Changes in Time–Activity Curve Dynamics with Development of Metastasis

To explore the changes in lymphatic flow on tumor implantation and metastasis development, dynamic ^{18}F-FDG lymphography was performed over the course of 4 wk after tumor implantation. The relative mean time–activity curve derived from the popliteal node on the tumor-bearing leg did not differ from the healthy control side within the first weeks of tumor growth. However, starting at week 2, subtle changes in the curves, with prolonged retention of ^{18}F-FDG in the diseased node, were already detectable (Fig. 3). In week 4, activity was retained during the entire scan, and markedly prolonged uptake into the node was evident. Regarding the corresponding CT images, enlargement of the node was evident only at week 4.

Cerenkov-Guided Metastasis Resection

The accumulated ^{18}F-FDG in popliteal lymph nodes after successful ^{18}F-FDG lymphography emits a detectable Cerenkov signal. The prolonged retention of ^{18}F-FDG in metastatic lymph nodes allowed for intraoperative differentiation of metastatic from healthy lymph nodes with Cerenkov imaging. Although a Cerenkov signal capable of guiding surgical excision was still evident within metastatic lymph nodes at approximately 1.5 h after injection, the contralateral exposed lymph nodes did not show any discernable Cerenkov signal at that time (Fig. 4). After excision of the respective nodes, no residual Cerenkov signal was detected within the popliteal lymph basins. H&E staining of the Cerenkov-positive node revealed metastatic infiltration (Fig. 4).

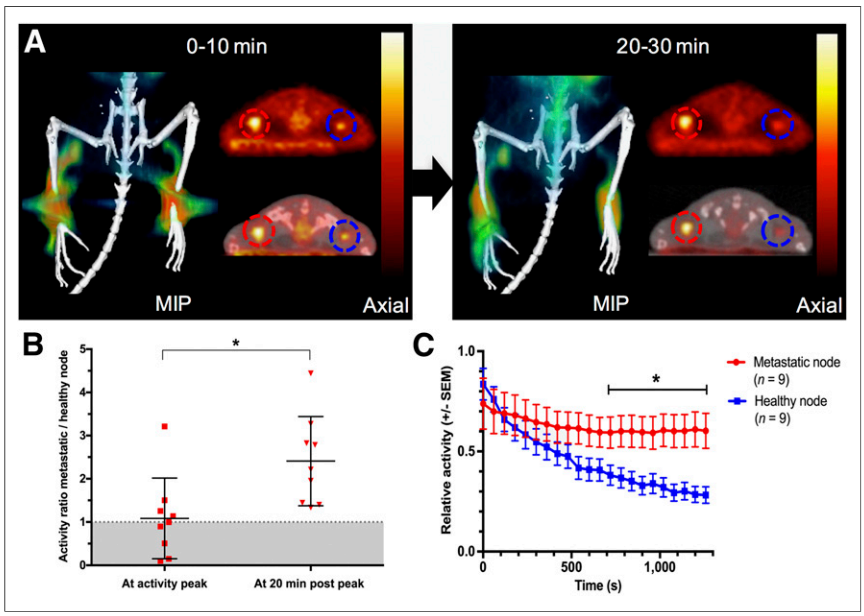

FIGURE 1. (A) Coronal maximum-intensity projection (MIP) and corresponding axial PET and fused PET/CT images derived from first 10 and last 10 min of 30-min dynamic ^{18}F-FDG lymphography scan. Prolonged retention of radioactivity is seen in metastatic (red circles) versus healthy (blue circles) popliteal lymph nodes after ^{18}F-FDG lymphography in mice implanted with B16F10 tumors on right hind paw. (B) Relative activity ratios between metastatic and healthy nodes are significantly higher 20 min after intraindividual peak uptake. (C) When displayed over time, longer retention of activity in metastatic nodes is evident, and from minute 13 after intraindividual peak uptake, relative activities remain significantly higher in metastatic nodes than in intraindividual healthy control nodes ($P < 0.05$).

Specificity for Metastatic Lymphadenopathy

To evaluate the described positron lymphography approach for cancer specificity, mice in which an acute inflammation known to cause inflammatory lymphadenitis had been induced in the right hind paw were examined repeatedly and used as a control. Mean relative activity ratios between the healthy side and the inflammatory or metastatic side 20 min after peak activity were evaluated. At 3 h after induction of inflammation, mean relative activity ratios between the intraindividual lymphadenopathy versus the healthy node were significantly higher in the metastatic model than in the inflammatory model (2.41 ± 1.03 [$n = 9$] vs. 1.37 ± 0.15 [$n = 4$]; $P < 0.05$). However, 24 h after the induction of inflammation in

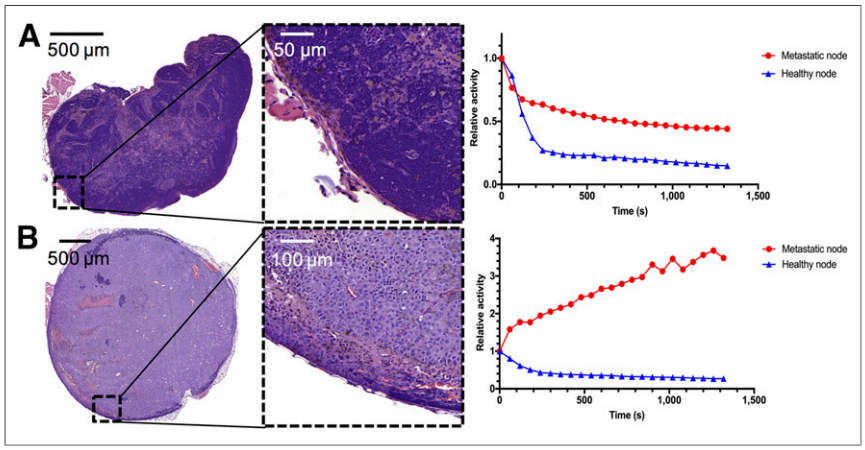

FIGURE 2. H&E staining and activity curves. (A) Results in mouse bearing only small melanoma cell infiltrates mainly on lymph node border on metastatic side. Activity curves in metastatic compared with healthy node tended to diverge in later scan minutes, showing retention effect in diseased node. (B) Results in mouse with large popliteal lymph node metastasis. Retention effect in diseased node is much higher, and only residual lymphatic tissue is preserved, as shown in H&E staining.

the same set of mice, the grouped mean activity ratio in the inflammatory model had more than doubled, resulting in no significant difference from the metastatic model (3.11 ± 0.30 vs. 2.41 ± 1.03; $n = 4$ vs. $n = 9$; $P > 0.05$). Thus, early inflammatory changes could be differentiated from metastasis, but at peak acute inflammation, differentiation of metastatic from inflammatory nodes based on their dynamics was not possible (Supplemental Fig. 2). After 120 h, with resolving inflammation, activity ratios at 20 min were lower again, with a mean value of about 1.5 in comparison to about 2.4 in metastatic mice; however, this finding was limited to a statistical trend (1.48 ± 0.75 vs. 2.41 ± 1.03; $n = 4$ vs. $n = 9$; $P = 0.07$).

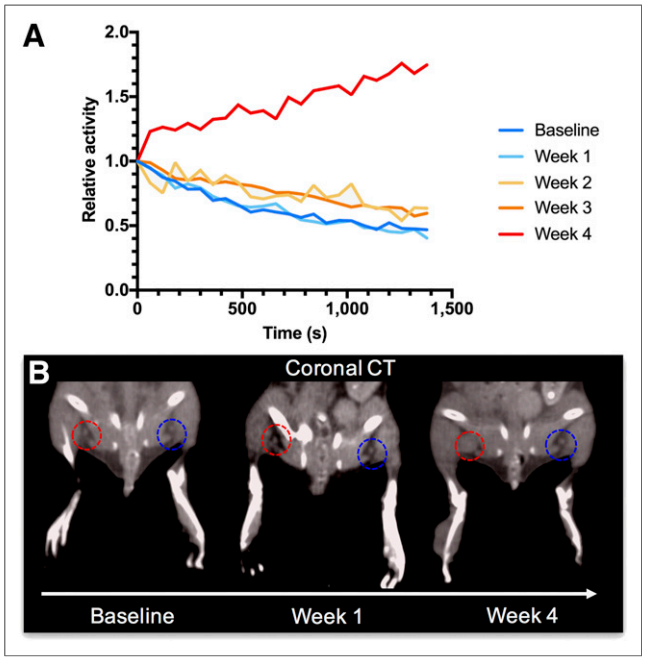

FIGURE 3. (A) When repeatedly imaged over 4 wk, alterations in lymphatic drainage become evident with developing metastasis in mouse. Tumor-draining popliteal nodes' drainage dynamics do not differ from healthy contralateral control at baseline and week 1 after tumor implantation. From second week, subtly elevated activity retention levels can already be detected, whereas markedly prolonged uptake is seen in fourth week after tumor implantation. (B) Fittingly, with growing metastasis in week 4, evidence of lymph node enlargement on tumor-bearing side (red circles) is seen on coronal CT scans, when compared with contralateral healthy control (blue circles). At baseline and in week 1, lymph node sizes do not differ visually between the two sides.

DISCUSSION

Sentinel lymph node resection and subsequent histopathologic analysis are part of the routine diagnostic workup in certain cancers such as melanoma, cervical cancer, and breast cancer. Lymphography using blue dye and lymphoscintigraphy techniques are currently inevitable for pre- and intraoperative sentinel lymph node diagnostics. Although extensively evaluated, routine uses of these techniques allow only for identification and localization of the sentinel lymph node, without providing further details about possible metastatic involvement. Using radiocolloids alone, the identification rate of the sentinel node has been reported to be fairly high, averaging approximately 94% and ranging from 67% to100% (*10*). However, since the approach itself is nonspecific and not tumor-targeted, the efficiency in detecting micrometastases strongly depends on the pathologist after sentinel lymph node excision and is prone to high false-negative rates. Hence, of patients undergoing the sentinel lymph node procedure, the approximate number in whom lymph node metastases are found is only 20% or less, resulting in a very high oversampling rate (*11–13*). Dynamic lymphography, especially in malignant melanoma, might serve as a possible marker in predicting metastatic spread, as lymphangiogenesis in tumor-draining nodes is promoted even before metastatic involvement occurs, and lymphatic drainage is already altered at early time points (*14–16*).

Positron lymphography using the small molecular tracer ^{18}F-FDG has already been shown to be feasible in healthy mice (*7*). In our study using a murine melanoma model, we found that during ^{18}F-FDG lymphography, lymph flow dynamics differ between metastatic nodes and healthy control nodes, even at early time points after induction of local inflammation. The radiotracer injected peritumorally and on the contralateral healthy hind paw showed fast drainage to the popliteal lymph nodes on both sides, but retention was longer in metastatic popliteal lymph nodes than in the intraindividual healthy control nodes, likely because of the underlying structural lymphatic changes promoting prolonged drainage into the node over time as well as the direct metabolism of ^{18}F-FDG by node-invading tumor cells. These alterations gradually developed over time with primary tumor growth and metastatic spread to the popliteal node and therefore might be of use not only simply to identify the sentinel lymph node but also to visualize concomitant changes in lymphatic drainage patterns under metastasis development and to get a first indication of metastatic node involvement in the same imaging session. In our study, even small melanoma cell infiltrates in the subcapsular zone of the lymph node, resembling micrometastasis, led to increased retention of ^{18}F-FDG per weight when compared with the respective healthy node. Using the same model, we found that intravenously administered diagnostic

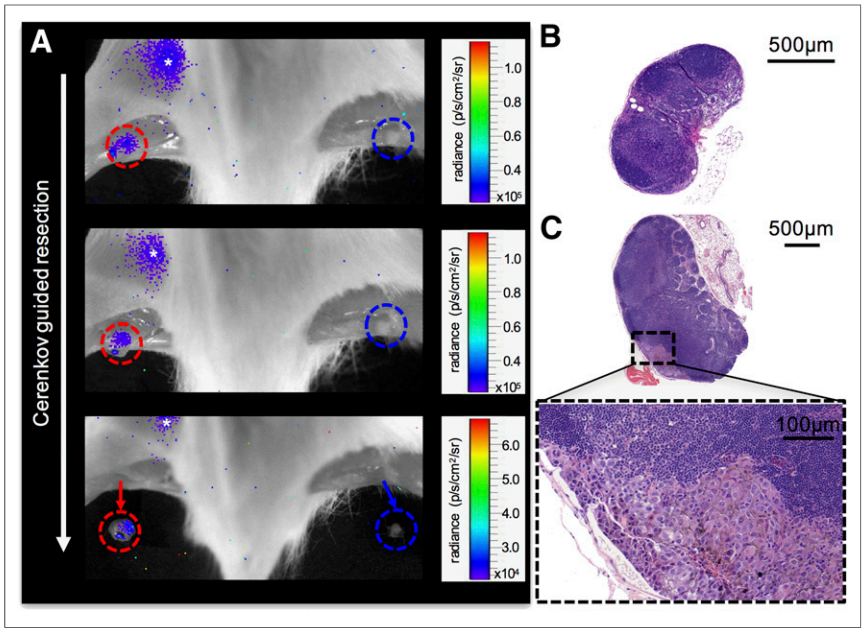

FIGURE 4. (A) ^{18}F-FDG lymphography images (tumor not in field of view, mouse positioned prone, fur and skin removed, acquisition time of 5 min) showing stepwise Cerenkov-guided resection of metastatic (red circles) popliteal lymph node and corresponding contralateral healthy control node (blue circles) of mouse implanted with B16F10 tumor on right hind paw. At 1.5 h after bilateral ^{18}F-FDG injection (3.7 MBq per side), metastatic node can still be identified by its subtle Cerenkov signal (mean signal-to-background ratio over time, 1.21 ± 0.14), whereas contralateral healthy control node does not show residual Cerenkov radiation (mean signal-to-background ratio over time, 0.69 ± 0.13), allowing for differentiation between the two and potential selective resection of tumor-bearing nodes. Asterisk indicates ^{18}F-FDG pooling in bladder. (B) Healthy, uninvolved node displayed for size comparison. (C) H&E staining provides evidence of metastatic involvement of tumor side of popliteal lymph node by melanin-containing cells.

^{18}F-FDG PET/CT was not sufficient to detect those lymphatic micrometastases (*5*). Additionally, we found that retention of relative activity normalized to weight was significantly correlated with the volume of metastatic nodes. Thus, we could identify nodes with rather small metastatic cell infiltrates and could already observe subtle changes in tracer dynamics in very early stages after tumor inoculation. In theory, a possible underlying explanation for this finding is initial lymphadenopathy due to early infiltration of immune cells (*15*) or tracer retention due to high lymphatic tracer delivery to the node with concomitant increased metabolism in initial melanoma cell infiltrates. Lacking a sufficient vascular network, very small lesions could possibly evade delineation on imaging studies with intravenous tracer delivery approaches, underlining the local route of administration proposed in our study.

Furthermore, the observed changes in tracer dynamics can be used for intraoperative optical imaging through Cerenkov luminescence and selective image-guided resection of metastatic nodes on the basis of their higher residual Cerenkov signal at later time points.

Our study faces certain limitations. First, ^{18}F-FDG is a sensitive yet very nonspecific radiopharmaceutical, showing significant uptake also in inflammatory lesions (*17,18*). This phenomenon also occurs during positron lymphography. Imaging results can therefore be interpreted only as a first diagnostic hint. However, inflammatory lymphangiogenesis resulting in promoted lymphatic drainage is reversible (*19*), and we observed uptake ratios 20 min after peak comparable to our metastatic model only in acute inflammation, whereas uptake ratios in early and resolving inflammation trended lower. To further evaluate the proposed approach and its potential clinical benefit, more specific radiotracers, such as *N*-(2-(diethylamino)ethyl)-2-^{18}F-fluoropropanamide, a novel radiotracer for imaging melanoma (*20*), could additionally be used in future studies. Yet, in a study on sentinel node mapping in patients using a melanoma-specific labeled monoclonal antibody probe for lymphoscintigraphy, no advantage was shown over a nonspecific radiocolloid; therefore, careful selection and prior evaluation of such probes and techniques remains crucial (*21*).

Furthermore, it is likely that the approach proposed in this study can significantly reduce the high oversampling rates of up to 80%–90% in current sentinel lymph node procedures that are based on the sole identification and extraction of the first draining lymph nodes in clinically node-negative patients irrespective of the tumor status. Oversampling may merely affect false-positive lymphadenopathic nodes, such as those that are false-positive because of inflammation in the direct tumor-draining lymph basin. It is not likely that any healthy nodes would be subject to extraction, potentially leading to a high positive predictive value for the proposed concept. Quantification of the predictive value and oversampling rates remains subject to further studies, which are under way.

When injected into tissue, ^{18}F-FDG shows fast diffusion into the vasculature, increasing systemic background activity. Intracutaneous injections in mice have been shown to lead to delayed systemic uptake (*7*). By comparison, the relatively early increase in systemic background observed in our study, with activity present in the bladder within the first 10 scan minutes, is most likely due to the high hydrostatic pressure within the tumor-bearing legs and the highly vascularized nature of B16F10 tumors. Despite the increased background, major draining lymph vessels and popliteal nodes were also clearly depicted at later scan time points that already exhibited systemic uptake. However, at later time points, tumor visualization was also possible, similar to a standard PET image. In mice, this allows one to use a single dose to perform first a positron lymphography scan and then a standard PET scan. It is important to keep in mind that in metastatic nodes, additional systemic radiotracer uptake due to their high glucose metabolism can further enhance the retention effect observed in positron lymphography, and our data do not allow for differentiation of the two. However, in positron lymphography the significantly decreased background allows for a facile identification of the nodes, whereas performing diagnostic intravenous ^{18}F-FDG PET/CT was not found to be suitable for the detection of micrometastases, as previously shown by our group using the same mouse model (*5*).

Looking at the direct clinical translatability of our approach, a first study on humans performing intracutaneous limb injections for lymphography has not seen lymphatic vasculature and draining lymph basins in the human leg (*22*). Thus, to account for differences in the lymphatic systems and function between rodents and humans and to conclusively assess feasibility and possible clinical

applications of the proposed technique, further trials in humans evaluating interstitial or intratumoral injections in different anatomic locations are necessary and currently under way (clinical trials identifier at clinicaltrials.gov: NCT02285192). The results will be reported separately. It is also important to note that similar to other studies (*23*) positron lymphography could be combined with optical imaging as well. To exemplify, we used Cerenkov luminescence imaging. However, for intraoperative use of Cerenkov imaging after ^{18}F-FDG administration, the long acquisition time and the significant signal attenuation by overlying tissue and its optical properties could be limiting and even more relevant in humans than in mice. Moreover, detectability will be dependent on the extent and location of metastatic growth within the node. The observed retained high uptake in metastatic lymph nodes as well as the distinct distribution of metastatic foci in the subcapsular regions of the lymph nodes (i.e., in superficial areas) in melanoma (*24*) can potentially compensate for this. Increasing systemic uptake might obscure visualization of the nodes, especially deep-tissue lymph nodes such as those near the urinary bladder. Also, the melanoma mouse model chosen for its reliable metastatic features in our study is not ideal for Cerenkov imaging, as the contained melanin might partly quench the signal and lower the signal intensity.

CONCLUSION

Significantly longer retention of ^{18}F-FDG during positron lymphography is seen in metastatic than nonmetastatic lymph nodes in a B16F10 mouse model, allowing for differentiation of the two and for the selective resection of tumor-bearing nodes using Cerenkov imaging.

DISCLOSURE

This work was supported by National Institutes of Health grants R01CA183953-01A1, R01EB014944 (Jan Grimm), and P30 CA08748 (Cancer Center Core Grant); by the Mr. William H. and Mrs. Alice Goodwin and the Commonwealth Foundation for Cancer Research; by the Center for Experimental Therapeutics of the Memorial Sloan Kettering Cancer Center (Jan Grimm); by a Society of MSKCC research grant (Jan Grimm); by a Heinrich Hertz-Stiftung Research Fellowship grant (Hannah Lockau); and by a Deutsche Forschungsgemeinschaft (DFG) Research Fellowship grant NE 1922/2-1 (Volker Neuschmelting). No other potential conflict of interest relevant to this article was reported.

ACKNOWLEDGMENTS

We thank Pat Zanzonico and Valerie Longo (MSKCC Small Animal Imaging Core Facility) for their technical support.

REFERENCES

1. Gershenwald JE, Thompson W, Mansfield PF, et al. Multi-institutional melanoma lymphatic mapping experience: the prognostic value of sentinel lymph node status in 612 stage I or II melanoma patients. *J Clin Oncol.* 1999;17:976–983.
2. Morton DL, Thompson JF, Cochran AJ, et al. Sentinel node biopsy or nodal observation in melanoma. *N Engl J Med.* 2006;355:1307–1317.
3. Tichauer KM, Samkoe KS, Gunn JR, et al. Microscopic lymph node tumor burden quantified by macroscopic dual-tracer molecular imaging. *Nat Med.* 2014;20:1348–1353.
4. Zhou Z, Qutaish M, Han Z, et al. MRI detection of breast cancer micrometastases with a fibronectin-targeting contrast agent. *Nat Commun.* 2015;6:7984.
5. Neuschmelting V, Lockau H, Ntziachristos V, Grimm J, Kircher MF. Lymph node micrometastases and in-transit metastases from melanoma: in vivo detection with multispectral optoacoustic imaging in a mouse model. *Radiology.* 2016;280:137–150.
6. Partridge SC, Kurland BF, Liu C-L, Ho RJY, Ruddell A. Tumor-induced lymph node alterations detected by MRI lymphography using gadolinium nanoparticles. *Sci Rep.* 2015;5:15641.
7. Thorek DLJ, Abou DS, Beattie BJ, et al. Positron lymphography: multimodal, high-resolution, dynamic mapping and resection of lymph nodes after intradermal injection of ^{18}F-FDG. *J Nucl Med.* 2012;53:1438–1445.
8. Thorek DLJ, Riedl CC, Grimm J. Clinical Cerenkov luminescence imaging of ^{18}F-FDG. *J Nucl Med.* 2014;55:95–98.
9. Rau FC, Weber WA, Wester HJ, et al. O-(2-[^{18}F]fluoroethyl)-L-tyrosine (FET): a tracer for differentiation of tumour from inflammation in murine lymph nodes. *Eur J Nucl Med Mol Imaging.* 2002;29:1039–1046.
10. Niebling MG, Pleijhuis RG, Bastiaannet E, Brouwers AH, Van Dam GM, Hoekstra HJ. A systematic review and meta-analyses of sentinel lymph node identification in breast cancer and melanoma, a plea for tracer mapping. *Eur J Surg Oncol.* 2016;42:466–473.
11. Landi G, Polverelli M, Moscatelli G, et al. Sentinel lymph node biopsy in patients with primary cutaneous melanoma: study of 455 cases. *J Eur Acad Dermatol Venereol.* 2000;14:35–45.
12. Wagner JD, Corbett L, Park HM, et al. Sentinel lymph node biopsy for melanoma: experience with 234 consecutive procedures. *Plast Reconstr Surg.* 2000; 105:1956–1966.
13. Morton DL, Thompson JF, Cochran AJ, et al. Final trial report of sentinel-node biopsy versus nodal observation in melanoma. *N Engl J Med.* 2014;370:599–609.
14. Qian CN, Berghuis B, Tsarfaty G, et al. Preparing the "soil": the primary tumor induces vasculature reorganization in the sentinel lymph node before the arrival of metastatic cancer cells. *Cancer Res.* 2006;66:10365–10376.
15. Harrell MI, Iritani BM, Ruddell A. Tumor-induced sentinel lymph node lymphangiogenesis and increased lymph flow precede melanoma metastasis. *Am J Pathol.* 2007;170:774–786.
16. Mumprecht V, Honer M, Vigl B, et al. In vivo imaging of inflammation- and tumor-induced lymph node lymphangiogenesis by immuno-positron emission tomography. *Cancer Res.* 2010;70:8842–8851.
17. Strauss LG. Fluorine-18 deoxyglucose and false-positive results: a major problem in the diagnostics of oncological patients. *Eur J Nucl Med.* 1996;23:1409–1415.
18. Shreve PD. Focal fluorine-18 fluorodeoxyglucose accumulation in inflammatory pancreatic disease. *Eur J Nucl Med.* 1998;25:259–264.
19. Mumprecht V, Roudnicky F, Detmar M. Inflammation-induced lymph node lymphangiogenesis is reversible. *Am J Pathol.* 2012;180:874–879.
20. Liu H, Liu S, Miao Z, et al. A novel aliphatic ^{18}F-labeled probe for PET imaging of melanoma. *Mol Pharm.* 2013;10:3384–3391.
21. Bartolomei M, Testori A, Chinol M, et al. Sentinel node localization in cutaneous melanoma: lymphoscintigraphy with colloids and antibody fragments versus blue dye mapping. *Eur J Nucl Med.* 1998;25:1489–1494.
22. Jensen MR, Simonsen L, Lonsdale M, Bülow JB. Foot skin depots of ^{18}F-fluorodeoxyglucose do not enable PET/CT lymphography of the lower extremity lymphatic system in man. *EJNMMI Res.* 2013;3:17.
23. KleinJan GH, Hellingman D, van den Berg NS, et al. Hybrid surgical guidance: does hardware integration of γ- and fluorescence imaging modalities make sense? *J Nucl Med.* 2017;58:646–650.
24. Murray CA, Leong WL, McCready DR, Ghazarian DM. Histopathological patterns of melanoma metastases in sentinel lymph nodes. *J Clin Pathol.* 2004; 57:64–67.